ACS OMEGA

Open Access



http://pubs.acs.org/journal/acsodf

Article

# Spectral Analysis of Bloch-Like Oscillations in Conjugated Polymers

Sutao Sun*

Cite This: *ACS Omega* 2023, 8, 40456−40462

Read Online

ACCESS | Metrics & More | Article Recommendations

**ABSTRACT:** We present a spectrum investigation of the behavior of dissociated polarons under high electric fields in conjugated polymers. The study employs the Su-Schrieffer−Heeger model along with nonadiabatic molecular dynamics and frequency-domain analysis methods to analyze the Bloch-like oscillations. It is found that the fundamental frequencies of the current density agree well with the theoretical Bloch frequencies of the perfect crystals. The electron−phonon coupling is a key factor in inducing the deviation between the Bloch-like oscillation behavior in conjugated polymers and that in perfect superlattices. Moreover, the increase in lattice thermal fluctuation is not conducive to the maintenance of Bloch-like oscillation behavior in conjugated polymers.

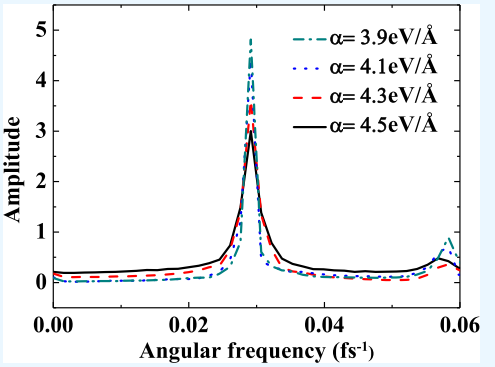


## 1. INTRODUCTION

Free electrons in a periodic lattice submit to a periodic potential oscillation behavior under a uniform electric field, and this phenomenon is called Bloch oscillations (BOs), which was first theoretically predicted by Bloch and Zener.[1] In fact, due to the real existence of lattice defects, impurities, and various scatters, the relaxation time of the electrons is much shorter than the period of BO, so BO is difficult to observe. It was not until 1993 that Waschke et al. observed BO for the first time in experiments with superlattice materials of inorganic semiconductors.[2] Since then, BOs have been intensively studied both experimentally and theoretically.[3−23]

In organic conjugated polymers, charged carriers dissociate and become free electrons under the control of a strong electric field. With the wide application of organic polymer materials in the field of optoelectronic devices, the dynamic properties of free carriers under an applied electric field have become a research topic.[24−33] Li et al. found that the dissociated polaron propagates in the form of a free-like electron and performs spatial BO. In contrast to normal BO in a rigid lattice, the mean displacement of the oscillating electron will have a net forward movement in the direction of the electric field.[24] Soon after, the BO of solitons in a deformable molecular chain was studied by Lakhno and Korshunova.[26] Their results showed that there exists a critical electric field value, $E_c$. If the field is lower than $E_c$, a soliton performs BO as a whole, while when the field is higher than $E_c$, the soliton turns into a breather and oscillates. Later on, e Silva et al.[27] studied the dynamics of a dissociated polaron in organic and inorganic polymers. They found that the critical electric field of charge BO in inorganic polymer chains is lower than that in organic polymer chains. Moreover, they believe that there is no drifting motion of charge.

Although beneficial theoretical and practical explorations have been made in the study of BO in conjugated polymers, there are still many questions that need further research, such as: Does charge-directional drift exist in the charge-like BO behavior? What are the differences between the BO in organic polymers and that in ideal lattices?

The author believes that it is no longer suitable to study the oscillating behavior of the electron by calculating and analyzing the stable velocity of the charge (or the central position of the charge) due to the periodically "instantaneous polaron state", while the oscillating charge performs spatial BO. In addition, the author also believes that the periodic oscillation behavior of electrons is more suitable for analysis and research in the frequency domain. In summary, in this paper, the dynamic behavior of dissociated polarons in organic polymer chains under a strong field is simulated by using the nonadiabatic molecular dynamics method, and then the Bloch-like oscillation behavior of free electrons is analyzed by using the frequency domain analysis method.

## 2. MODEL AND NUMERICAL METHOD

**2.1. Model and Molecular Dynamics.** The SSH model[34] with a Brazovskii−Kirova-type symmetry-breaking term has been used and written as

Received: July 14, 2023
Accepted: October 6, 2023
Published: October 17, 2023

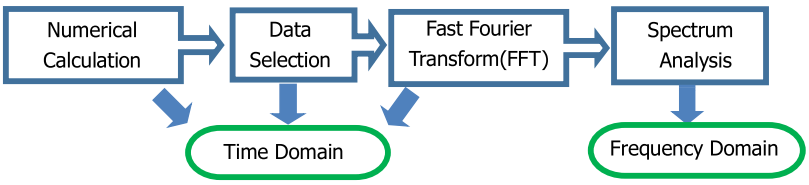


**Figure 1.** Main steps of spectrum calculation.

$$H = -\sum_n t_n(e^{-i\gamma A}a_{n+1}^{\dagger}a_n + e^{i\gamma A}a_n^{\dagger}a_{n+1}) + \frac{1}{2}\beta\sum_n (u_{n+1}-u_n)^2 + \frac{M}{2}\sum_n \dot{u}_n^2 \quad (1)$$

here, $t_n = [t_0 - \alpha(u_{n+1} - u_n) - (-1)^n t_e]$ is the hopping matrix element, with $t_0$ being the transfer integral of electrons in a regular lattice, $\alpha$ is the electron−lattice coupling constant, and $u_n$ is the lattice displacement of site $n$ from its undimerized equilibrium position. The term $t_e$ is introduced to lift the ground-state degeneracy in nondegenerate polymers.[35] $\gamma \equiv ea/(\hbar c)$, with $e$, $a$, and $c$ being electron charge, lattice constant, and speed of light, respectively. Vector potential $A(t)$[36] is introduced to describe an electric field within the periodic boundary conditions and is related to the external electric field through $E(t) = -(1/c)\partial A/\partial t$. $E(t)$ is turned on in the form of a linear function, that is, $E(t) = (E_0/t_c)\cdot t$ for $0 < t < t_c$, and $E(t) = E_0$ for $t > t_c$, with $t_c = 50$ fs or all the results shown below. $a_{n+1}^{\dagger}(a_n^{\dagger})$ is the creation (annihilation) operator that creates (annihilates) an electron at site $n$. $\beta$ is the elastic constant, and $M$ is the mass of a CH group.

We assume that there is a static polaron in the system for $t < 0$ and that the external electric field is applied for $t > 0$. The static polaron solution is obtained by solving the self-consistent equation for $y_n$, which is written as

$$y_n = u_{n+1} - u_n = \frac{2\alpha}{N\beta}\sum_n \sum_i^{\text{occu.}} \varphi_i(n+1)\varphi_i(n) - \frac{2\alpha}{\beta}\sum_i^{\text{occu.}} \varphi_i(n+1)\varphi_i(n) \quad (2)$$

where $\varphi_i$ is the eigenfunction diagonalizing the electronic Hamiltonian with $A(t) = 0$; in this case, the eigenfunctions can be taken as real functions. The sum over $n$ is restricted to the occupied states. The periodic boundary condition has been used, and an extra condition $\sum_n (u_{n+1} - u_n) = 0$ is added to guarantee that the polymer chain length remains unchanged. $N$ is the number of CH units in the system we are considering.

Once the initial lattice configuration $u_n$ and the electron distribution $\varphi_i$ are determined, then the lattice configuration at any time $t$ ($t > 0$) can be obtained by the equation of motion for the atomic displacements

$$M\ddot{u}_n(t) = -\beta[2u_n(t) - u_{n+1}(t) - u_{n-1}(t)] + \alpha\{e^{i\gamma A}[\rho_{n-1,n}(t) - \rho_{n,n+1}(t)] + e^{-i\gamma A}[\rho_{n,n-1}(t) - \rho_{n+1,n}(t)]\} - \lambda M\dot{u}_n + f_n(t) \quad (3)$$

where the density matrix $\rho_{n,n'}(t) = \sum_\nu \psi_\nu^*(n,t) f_\nu \psi_\nu(n',t)$, with $f_\nu = (0,1 \text{ or } 2)$ being the time-independent distribution function, is determined by the initial electron occupation. The last two terms of eq 3 describe the thermal effects. $\lambda = (0.001\ \text{fs}^{-1}$ in the simulation) is the friction constant. $f_n(t)$ is a thermal random force having the following statistical properties:[37,38] $\langle f_n(t)\rangle \equiv 0$ and $\langle f_n(t) f_{n'}(t')\rangle = 2\kappa_B T M\lambda\delta(t-t')$, where $\kappa_B$ is the Boltzmann constant and $T$ is the temperature.

The evolution of the electronic stage with time is obtained by solving the time-dependent Schrödinger equation

$$i\hbar\dot{\psi}_\nu(n,t) = -t_n e^{-i\gamma A}\psi_\nu(n+1,t) - t_{n-1}e^{i\gamma A}\psi_\nu(n-1,t) \quad (4)$$

The calculations of coupled differential eqs 3 and 4 were carried out by a standard fourth-order Runge−Kutta numerical[39] method. The results considering the temperature effects shown below have been taken as the ensemble average over 20 simulations.

The parameters used here are taken as those appropriate for polyacetylene,[24] i.e., $t_0 = 2.5$ eV, $t_e = 0$−$0.45$ eV, $\alpha = 4.1$ eV/Å, $\beta = 21.0$ eV/Å$^2$, $M = 1349.14$ eV·fs$^2$/Å$^2$, and $a = 1.22$ Å.

In this paper, we would like to investigate the spectral characteristics of dissociated polaron dynamics using the bond-current density[40]

$$j_n(t) = -\frac{2|e|}{\hbar}\text{Im}(t_{n,n+1}c_{n+1}^{\dagger}c_n) \quad (5)$$

The stability of the dissociated polaron profile can be estimated by using the localization length

$$l_{\text{loc}} = 1/\sum_{n=1}^{N}\psi_\nu^4(n) \quad (6)$$

here, small values of $l_{\text{loc}}$ correspond to highly localized polaron profiles, and high values of $l_{\text{loc}}$ describe the extended states.

**2.2. Spectral Analysis Method.** The data processing steps of the spectral analysis method are shown in Figure 1. It mainly consists of four steps: numerical calculation, data selection, fast Fourier transform (FFT), and spectrum analysis. The first three steps are performed in the time domain, and the fourth step is performed in the frequency domain. The function of each step is described as follows.

Step 1: Numerical calculation. In this step, the discrete-time data sequences of localization length $l_{\text{loc}}$ and current density $j_n$ can be obtained by solving the real-time evolution eqs 2−6 in Section 2.1.

Step 2: Data selection. In order to obtain typically sharp peaks in the frequency domain, the sampling of each segment is performed with a sampling rate $L = 2^{13}$. Moreover, it is worth mentioning that the components during the accelerating stage of the polaron velocity and the dissociating stage of the polaron in the first period are not considered; only the data when $t > 2t_c$ in the process of dynamic evolution are collected.

Step 3: Fast Fourier transform. According to the Wiener−Khinchin theorem, the spectra $A(\omega)$ of $\xi(\eta)(l_{\text{loc}}$ or $j_n)$ can be obtained by doing a fast Fourier transform (FFT).[41]



https://doi.org/10.1021/acsomega.3c05078
ACS Omega 2023, 8, 40456−40462

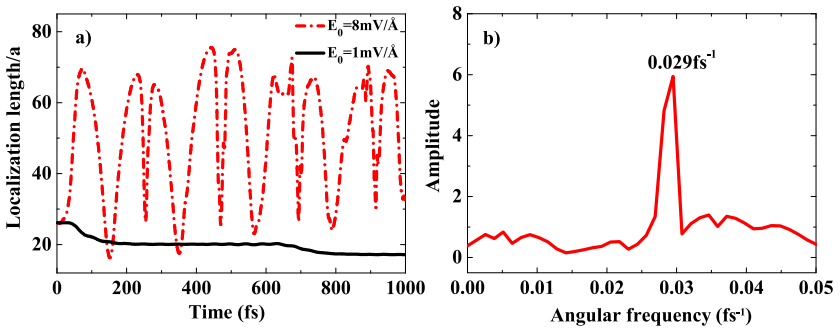


**Figure 2.** (a) Evolution of polaron localization and the (b) amplitude spectrum distribution under the electric field $E_0$ = 8 mV/Å.

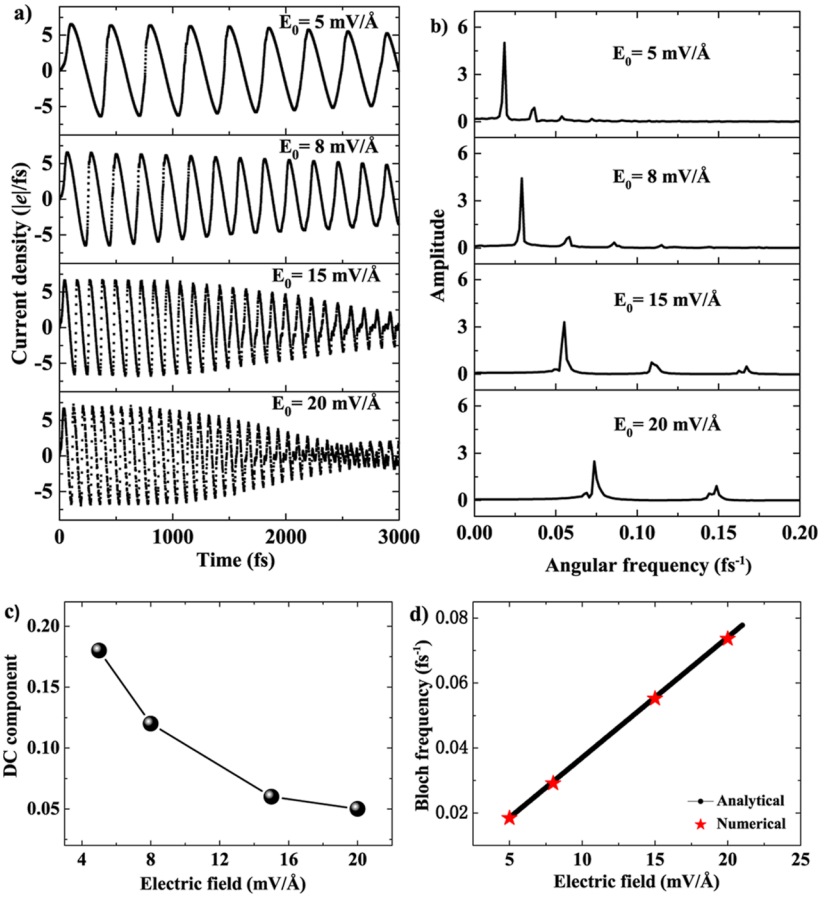


**Figure 3.** (a) Evolution of current density under four electric fields; (b) the amplitude spectrum distribution curves of current under four electric fields; (c) DC component as a function of the electric field; and (d) Bloch frequency as a function of the electric field.

$$A(\omega) = \sum_{\eta} \xi(\eta) e^{-i\omega\eta/L} \qquad (\eta = 1,2,3, \cdots, L-1) \tag{7}$$

Step 4: Spectrum analysis. $A(\omega)$ gives the amplitude variations with respect to the angular frequency $\omega$. A better understanding of the oscillatory characteristics of electron motion can be obtained by using $A(\omega)$.

## 3. RESULTS AND DISCUSSION

In numerical calculations, a polymer chain containing 200 CH units is considered. Initially, a negative polaron is located at the center of the chain. We are now in a position to numerically study the localization length, $l_{loc}$, of the polaron. Figure 2a shows the time evolution of the $l_{loc}$ under electric fields of 1 and 8 mV/Å. From the figure, one can see that, for the lower electric field, 1 mV/Å, the polaron moves with the lattice distortion accompanying the charge, and the $l_{loc}$ is about 25a in the beginning and then decreases slowly. However, for the higher electric field, 8 mV/Å, the $l_{loc}$ is dramatically different from the above case. In this case, the $l_{loc}$ increases sharply and up to 70a at around $t$ = 80 fs, which indicates that the polaron completely dissociates. Two points are worth mentioning over our simulation time: 1) the $l_{loc}$ presents an oscillatory behavior and 2) a series of transient self-trapping states are observed at the end of every period. To gain a better understanding of the oscillatory behavior of the $l_{loc}$, we calculated the amplitude spectrum of the $l_{loc}$ by $A(\omega) = \sum_{\eta} l(\eta) e^{-i\omega\eta/L}$, as shown in Figure 2b. The results show that the oscillatory frequency of the $l_{loc}$ is 0.029 $fs^{-1}$, which agrees well with the frequency of BO in a homogeneous lattice (the period $\tau_B = \frac{h}{eE_0 d}$ with $h$, $e$, $E_0$, and $d$



https://doi.org/10.1021/acsomega.3c05078
ACS Omega 2023, 8, 40456−40462

being the Planck's constant, electron charge, applied electric field, and the period of the lattice, respectively, the frequency $\omega_B = \frac{2\pi}{\tau_B}$).[1]

To gain a better understanding of the BO of a dissociated polaron under a high uniform electric field, in the following calculations we will calculate the time evolution and the amplitude spectrum distribution curves of $j = \sum_n j_n$ in the field range of $5 < E_0 < 20$ mV/Å. Four representative cases under the electric field $E_0$ = 5, 8, 15, and 20 mV/Å were selected for analyses in detail, which are presented in Figure 3. It is clear that, in all cases of Figure 3a, the $j$ exhibits spatial BO, and the period of the $j$ decreases with the increasing electric field. Another point to be noted is that, at about 1000 fs, the BO of $j$ gradually becomes a damped oscillation. And the stronger the electric field, the faster the current amplitude dampens. This indicates that the phonon scattering increases with the increasing electric field. In Figure 3b, the amplitude spectrum distribution curves of $j$ under four electric fields are shown. One can see that a series of well-separated sharp characteristic peaks are clearly observed. In addition, we find that the DC component of $j$ varies with the electric field. For a detailed analysis of these characteristic frequencies, Table 1 gives the DC component and the main

**Table 1. Main Characteristic Frequencies of Current Density under the Electric Fields $E_0$ = 5, 8, 15, and 20 mV/Å**

| $E_0$ (mV/Å) | DC (\|e\|/fs) | $\omega_1$ (fs$^{-1}$) | $\omega_2$ (fs$^{-1}$) | $\omega_3$ (fs$^{-1}$) |
|---|---|---|---|---|
| 5 | 0.18775 | 0.018408 | 0.036816 | 0.053689 |
| 8 | 0.1239 | 0.029146 | 0.058291 | 0.085903 |
| 15 | 0.06782 | 0.055223 | 0.10891 | 0.1672 |
| 20 | 0.05424 | 0.073631 | 0.1488 | 0.22243 |

characteristic frequencies of $j$ under four electric fields, in which $\omega_1$ corresponds to the fundamental frequency and $\omega_2$–$\omega_3$ are the harmonic frequencies. Meanwhile, Figure 3c,d shows the DC component and the fundamental frequency of $j$ as a function of the electric field. Obviously, as seen in Figure 3c, the drift motion of the charge carrier in the organic polymer does exist, which corresponds to the DC component of $j$. Also, the drift motion is steadily weakening with the increasing electric field. It indicates that the increasing electric field leads to the DC component of total current density becoming smaller and the component of alternating current becoming larger. From Figure 3d, it can be seen that the values of the fundamental frequencies $\omega_1$ are close to the theoretical Bloch frequency in perfect crystals. The frequency doubling is generally due to the nonlinear factor of the system.

It is widely known that the BO in a perfect lattice is a set of curves similar to positive/cosine in the time domain and a set of Dirac function curves in the frequency domain, as shown in Figure 4. Through the above analysis, we conclude that there is one similarity and four differences between the BO in an organic polymer and that in a perfect lattice. The similarity is that the BO frequency in the perfect lattice matches the fundamental frequency in the organic polymer numerically. The four differences are as follows: First, the amplitude of BO in the organic polymer attenuates over time; second, there is a directional drift of electrons in the BO in the organic polymer; third, the existence of the half-height width of the fundamental frequency peak of BO (hwBO) indicates the deviation of the BO in the organic polymer from that in the perfect lattice, and the larger the value of hwBO, the more it deviates from the BO in the

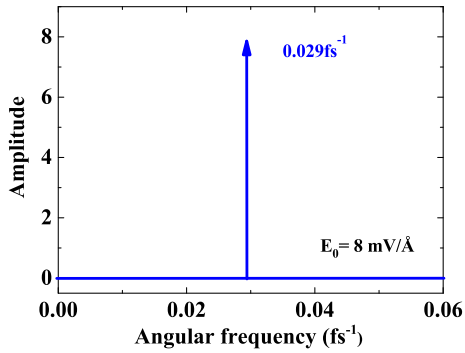


**Figure 4.** Bloch spectrum distribution in perfect lattices.

perfect lattice, which corresponds to the attenuation of the total current oscillation amplitude in the time domain; and finally, the existence of nonlinear factors in organic polymers leads to the existence of double and triple frequencies of BO frequencies in them.

To further elaborate on the BO in conjugated polymers, we will discuss the time evolution and the amplitude spectrum distribution curves of $j$ as affected by the electron–phonon (e–ph) coupling, which is important for gaining a better understanding of the BO in conjugated polymers. Figure 5a shows current density $j$ as a function of time for four different e–ph couplings. From the figure, one can see that the polaron dissociation is delayed with increasing e–ph couplings. This is because the polaron is a kind of quasiparticle with charge coupled to the lattice, and with the enhancement of e–ph couplings, the lattice's binding to charge further increases. As time goes by, the electron velocity becomes zero at the Brillouin boundary, and the total current density of the system reaches its maximum. At the same time, the maximum amplitude of the $j$ decreases with increasing e–ph couplings, such as 3.9 eV/Å, and the maximum amplitude of the $j$ is about 7 |e|/fs, while 5 |e|/fs for 4.5 eV/Å. As time goes on, another obvious feature one can get is that in all cases of Figure 5a, although the oscillatory amplitude of the $j$ decreases with time, the tendencies are different for different e–ph couplings. For weak e–ph couplings, such as 3.9 eV/Å, the $j$ decreases slowly within 3000 fs, while for the strong e-ph couplings, such as 4.5 eV/Å, the $j$ decreases remarkably, and when $t$ = 3000 fs, the amplitude of the $j$ is only about 3|e|/fs. This indicates that the phonon scattering increases with the increasing e–ph couplings. As the e–ph couplings of the system increase, the loss of electronic energy increases in the process of electrons interacting with the lattice, that is, the phonon scattering increases, which results in the total current density decaying faster with the enhancement of e–ph couplings. Then, we turn to the discussion of $j$ in the frequency domain. In Figure 5b, the DC component of $j$ as a function of the e–ph coupling is presented. It can be seen that the DC component of $j$ increases with an increasing e–ph coupling. This indicates that the drift velocity of the charge carrier is higher for stronger e–ph couplings. In Figure 5c, the characteristic peaks of $j$ for four different e–ph couplings are shown. One can see that the values of the fundamental frequency of $j$ ($\omega_1$) are nearly the same for all cases, which agree well with the frequency of BO in a homogeneous lattice, but the hwBO increases with increasing e–ph coupling. The increasing hwBO corresponds to the decreasing oscillatory amplitude of $j$, which is all caused by the higher phonon scattering in the condition of the stronger e–ph coupling.


https://doi.org/10.1021/acsomega.3c05078
ACS Omega 2023, 8, 40456–40462

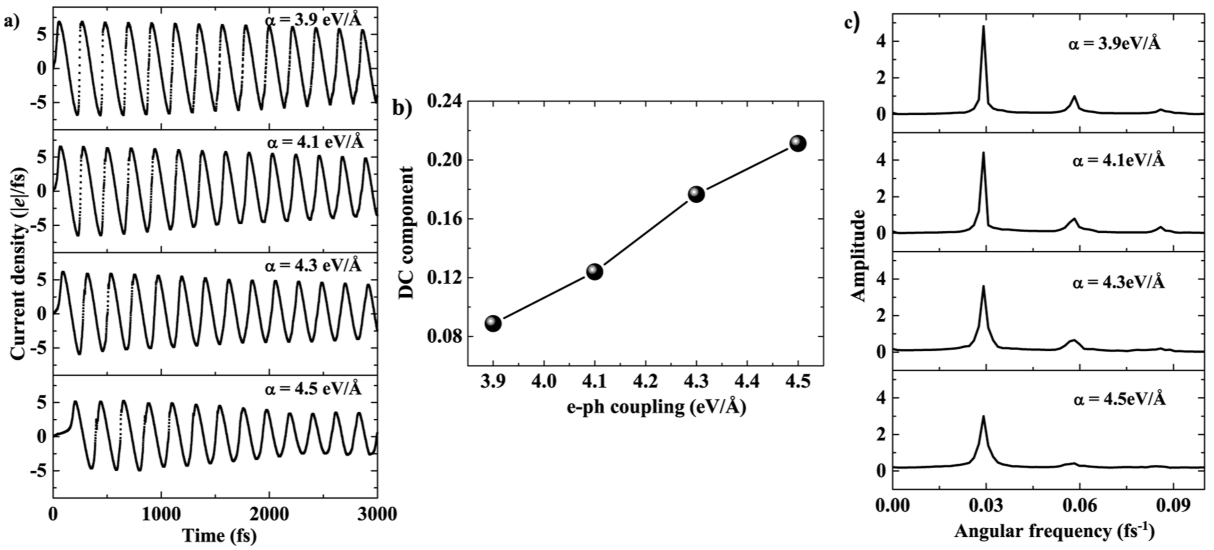


**Figure 5.** (a) Evolution of current density for four e-ph couplings; (b) DC component versus the e-ph coupling; and (c) the amplitude spectrum distribution curves of current density for four e-ph couplings. In all figures, $E_0$ = 8 mV/Å.

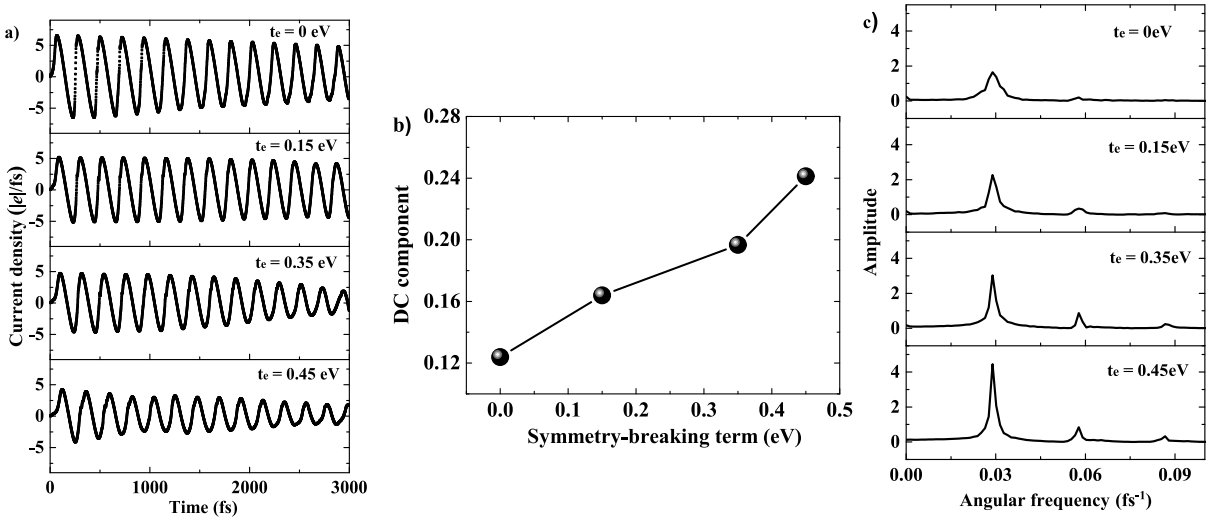


**Figure 6.** (a) Evolution of current density for four parameters $t_e$ ; (b) DC component versus the parameters $t_e$; and (c) the amplitude spectrum distribution curves of current density for parameters $t_e$. In all figures, $E_0$ = 8 mV/Å.

The symmetry-breaking term, $t_e$, not only reduces the stabilization velocity before polaron dissociation but also affects the total current density of the system after polaron dissociation. Figure 6a shows the evolution of current density for four parameters $t_e$ = 0, 0.15, 0.35, and 0.45 eV. One can see that the polaron dissociation is delayed with increasing $t_e$. At the same time, the maximum amplitude of $j$ decreases with increasing $t_e$, similar to Figure 5a. Figure 6b shows the DC component of $j$ as a function of $t_e$, and it can be seen that the DC component of $j$ increases with increasing $t_e$. In other words, with the increase in $t_e$, the difference between the displacement of the charge along the electric field direction and the displacement against the electric field direction increases. This also indicates that the drift velocity of the charge carrier is higher for stronger $t_e$. In Figure 6c, the characteristic peaks of the $j$ for four different $t_e$ values are shown. It is clear that the values of the fundamental frequency of current density $\omega_1$ are nearly the same for all cases, which agree well with the frequency of the BO in a homogeneous lattice. However, the difference is that with the increase of $t_e$, the hwBO gradually becomes wider, which is similar to that in Figure 5c. It shows that with the increase of $t_e$, the phonon scattering of the system is intensified, and the deviation of the BO in the organic polymer from that in the perfect lattice increases.

Previous results have shown that thermal oscillations of the lattice can reduce the carrier dissociation electric field.[42] Therefore, the effect of temperature on charge-like BO in organic polymers is studied, and the results of all calculations are the average values of 20 times. Figure 7a shows the real-time evolution of the total current density of the system at $T$ = 0, 5, 25, 50, and 150 K under the electric field $E_0$ = 8 mV/Å. As can be seen from the figure, with the increase in temperature, the stability of the oscillating current is gradually destroyed. When the system temperature is very low (less than 5 K), the attenuation of the total current density oscillation amplitude is weak. When the temperature of the system reaches 25 K, the amplitude attenuation of the oscillating current becomes quite obvious. When the temperature of the system rises to 50 K, the oscillation curve of the total current density becomes no longer


https://doi.org/10.1021/acsomega.3c05078
ACS Omega 2023, 8, 40456−40462

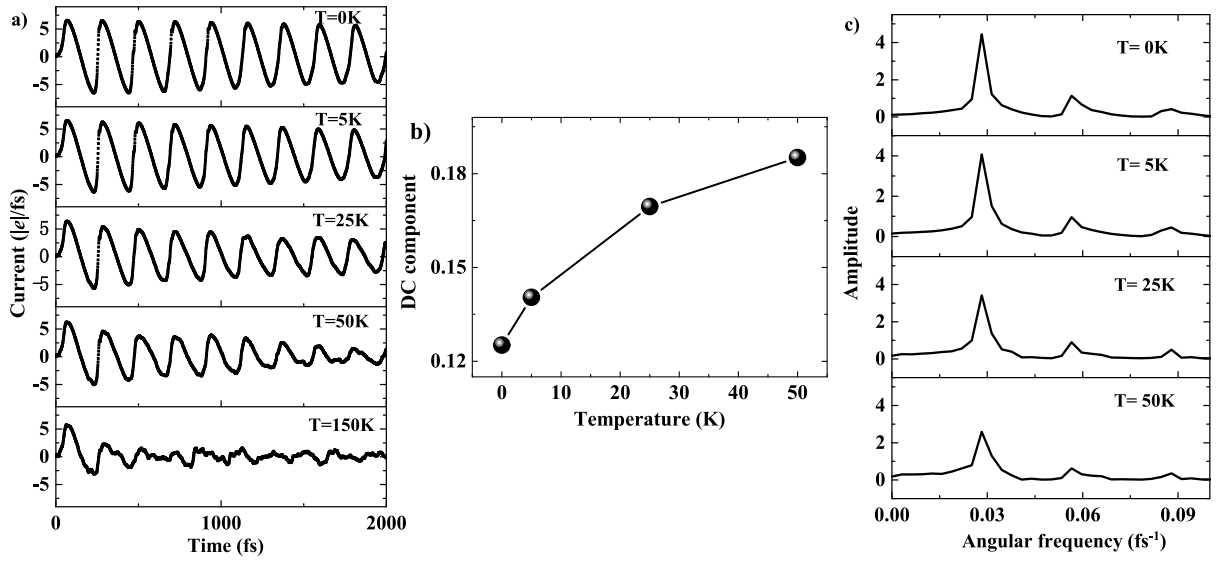


**Figure 7.** (a) Evolution of current density as a function of temperature; (b) DC component as a function of temperature; and (c) the amplitude spectrum distribution curves of current density as a function of temperature. In all figures, $E_0$ = 8 mV/Å.

smooth from 1500 fs, which indicates that the lattice heat fluctuation inhibits the BO of charge. When the temperature of the system rises to 150 K, the BO of the total current density lasts less than one cycle and is destroyed by the oscillation behavior of the lattice. At the same time, the BO of the total current density disappears. It reflects the competition mechanism between the electric field and temperature on the BO behavior in conjugated polymers. When the system temperature is higher than 150 K, the influence of lattice thermal vibration on the BO behavior is greater than that of the applied electric field.

Figure 7b shows the change of DC component of *j* with the temperature of the system under the action of the electric field, 8.0 mV/Å. It can be seen that with the increase of lattice heat fluctuation, the directional drift movement of charge slightly accelerates. This shows that the thermal oscillation of the lattice makes the DC component of the total current density slightly increase. Under the action of lattice thermal vibration, the difference between the charge displacement along the electric field direction and the charge displacement along the opposite electric field direction increases. Figure 7c shows the change of the amplitude spectrum of *j* with temperature. It can be seen that when the system temperature is lower than 50 K, the frequency of the Bloch-like oscillation of the total current density remains unchanged, but hwBO becomes wider with the increase of temperature. This shows that the existence of lattice thermal fluctuations is not conducive to the maintenance of charge-like BO behavior in organic polymers. The higher the temperature of the system, the more the BO deviates from that in the perfect lattice.

## 4. CONCLUSIONS

In this paper, the transport of a dissociated polaron in organic one-dimensional lattices is investigated using frequency-domain analysis methods. Under a strong field, a preexisting polaron breaks down quickly and exhibits BO behavior. The fundamental frequency of the current density numerically matches the BO frequency in a perfect lattice. However, there is a directional drift of electrons in the BO in an organic polymer, and also, the existence of the half-height width of the fundamental frequency peak of BO indicates the deviation of the BO in the organic polymer from that in the perfect lattice. The findings offer valuable insights into the maintenance and deviation of BO behavior in conjugated polymers.

## AUTHOR INFORMATION

### Corresponding Author

**Sutao Sun** − *School of Mathematics and Science, Hebei GEO University, Shijiazhuang 050031, China;* orcid.org/0000-0002-7709-8742; Email: sunsutao@126.com

Complete contact information is available at: https://pubs.acs.org/10.1021/acsomega.3c05078

### Notes

The author declares no competing financial interest.

## ACKNOWLEDGMENTS

The authors would like to thank the editor and the reviewers for their useful feedback that improved this paper.

## REFERENCES

(1) Bloch, F. Uber die Quantenmechanik der Elekronen in Kristallgittern. *Z. Phys.* **1929**, *52*, 555−600.

(2) Waschke, C.; Roskos, H. G.; Schwedler, R.; Leo, K.; Kurz, H.; Köhler, K. Coherent submillimeter-wave emission from Blochoscillations in a semiconductor Superlattice. *Phys. Rev. Lett.* **1993**, *70*, 3319−3322.

(3) Feldmann, J.; Leo, K.; Shah, J.; Plessen, G. V.; Thomas, P.; Rink, S. S.; Cunningham, J. Optical investigation of Bloch oscillations in asemiconductor superlattice. *Phys. Rev. B: Condens. Matter Mater. Phys.* **1992**, *46*, 7252−7257.

(4) Dekorsy, T.; Leisching, P.; Köhler, K.; Kurz, H. Electro-optic detection of Bloch oscillations. *Phys. Rev. B: Condens. Matter Mater. Phys.* **1994**, *50*, 8106−8109.

(5) Dekorsy, T.; Ott, R.; Kurz, H.; Köhler, K. Bloch oscillations at room temperature. *Phys. Rev. B* **1995**, *51*, 17275−17278.

(6) Unterrainer, K.; Keay, B. J.; Wanke, M. C.; Allen, S. J.; Leonard, D.; Medeiros-Ribeiro, G.; Bhattacharya, U.; Rodwell, M. J. W. Inverse Bloch Oscillator:Strong Terahertz-Photocurrent Resonances at the Bloch Frequency. *Phys. Rev. Lett.* **1996**, *76*, 2973−2976.

(7) Lyssenko, V. G.; Valušis, G.; Löser, F.; Hasche, T.; Leo, K.; Dignam, M. M.; Köhler, K.; Köhler, K. Direct Measurement of the

Spatial Displacement of Bloch-Oscillating Electrons in Semiconductor Superlattices. *Phys. Rev. Lett.* **1997**, *79*, 301−304.
(8) Zener, C. A Theory of the Electrical Breakdown of Solid Dielectric. *Proc. R. Soc.* **1934**, *145*, 523−529.
(9) Dignam, M.; Sipe, J. E.; Shah, J. Coherent excitations in the Stark ladder: Excitonic Bloch oscillations. *Phys. Rev. B* **1994**, *49*, 10502−10513.
(10) Sokolov, A. P.; Steffen, W.; Rossler, E. High-temperature dynamics in glass-forming liquids. *Phys. Rev. E* **1995**, *52*, 5105−5109.
(11) Ghosh, A. W.; Jönsson, L.; Wilkins, J. W. Bloch Oscillations in the Presence of Plasmons and Phonons. *Phys. Rev. Lett.* **2000**, *85*, 1084−1087.
(12) Domínguez-Adame, F.; Malyshev, V. A.; de Moura, F. A. B. F.; Lyra, M. L. Bloch-Like Oscillations in a One-Dimensional Lattice with Long-Range Correlated Disorder. *Phys. Rev. Lett.* **2003**, *91*, 197402.
(13) De Moura, F. A. B. F.; Lyra, M. L.; Domínguez-Adame, F.; Malyshev, V. A. Bloch oscillations in an aperiodic one-dimensional potential. *Phys. Rev. B* **2005**, *71*, 104303.
(14) Marder, M. P. *37 Condensed Matter Physics*; Wiley: New York, 2000, p 37.
(15) Ben Dahan, M.; Peik, E.; Reichel, J.; Castin, Y.; Salomon, C. Bloch Oscillations of Atoms in an Optical Potential. *Phys. Rev. Lett.* **1996**, *76*, 4508−4511.
(16) Morsch, O.; Müller, J. H.; Cristiani, M.; Ciampini, D.; Arimondo, E. Bloch Oscillations and Mean-Field Effects of Bose−Einstein Condensates in 1D Optical Lattices. *Phys. Rev. Lett.* **2001**, *87*, 140402.
(17) Sapienza, R.; Costantino, P.; Wiersma, D.; Ghulinyan, M.; Oton, C. J.; Pavesi, L. Optical Analogue of Electronic Bloch Oscillations. *Phys. Rev. Lett.* **2003**, *91*, 263902.
(18) Citrin, D. S. Magnetic Bloch Oscillations in Nanowire Superlattice Rings. *Phys. Rev. Lett.* **2004**, *92*, 196803.
(19) Wilkinson, S. R.; Bharucha, C. F.; Madison, K. W.; Niu, Q.; Raizen, M. G. Observation of Atomic Wannier-Stark Ladders in an Accelerating Optical Potential. *Phys. Rev. Lett.* **1996**, *76*, 4512−4515.
(20) Anderson, B. P.; Kasevich, M. A. Macroscopic Quantum Interference from Atomic Tunnel Arrays. *Science* **1998**, *282*, 1686−1689.
(21) Agarwal, V.; del Río, J. A.; Malpuech, G.; Zamfirescu, M.; Kavokin, A.; Coquillat, D.; Scalbert, D.; Vladimirova, M.; Gil, B. Photon Bloch Oscillations in Porous Silicon Optical Superlattices. *Phys. Rev. Lett.* **2004**, *92*, 097401.
(22) Sanchis-Alepuz, H.; Kosevich, Y. A.; Sánchez-Dehesa, J. Acoustic Analogue of Electronic Bloch Oscillations and Resonant Zener Tunneling in Ultrasonic Superlattices. *Phys. Rev. Lett.* **2007**, *98*, 134301.
(23) He, Z. J.; Peng, S. S.; Cai, F. Y.; Ke, M. Z.; Liu, Z. Y. Acoustic Bloch oscillations in a two-dimensional phononic crystal. *Phys. Rev. E* **2007**, *76*, 056605.
(24) Li, Y.; Liu, X. J.; Fu, J. Y.; Liu, D. S.; Xie, S. J.; Mei, L. M. Bloch oscillations in a one-dimensional organic lattice. *Phys. Rev. B: Condens. Matter Mater. Phys.* **2006**, *74*, 184303.
(25) Ribeiro, L. A., Jr.; Ferreira da Cunha, W.; Magela e Silva, G. Bipolaron assisted Bloch-like oscillations in organic lattices. *Phys. Lett. A* **2017**, *381*, 1915−1919.
(26) Lakhno, V. D.; Korshunova, A. N. Bloch oscillations of a soliton in a molecular chain. *Eur. Phys. J. B* **2007**, *55*, 85−87.
(27) Ribeiro, L. A.; da Cunha, W. F.; de Almeida Fonseca, A. L.; e Silva, G. M. Bloch oscillations in organic and inorganic polymers. *J. Chem. Phys.* **2017**, *146*, 144903.
(28) Liu, W. Research on Charge Transport in One-Dimensional Organic Semiconductors Material. *Adv. Mater. Res.* **2012**, *531*, 231−234.
(29) Nazareno, H.; Brito, P. d. Bloch oscillations as generators of polarons in a 1D crystal. *Physica B* **2016**, *494*, 1−6.
(30) Golez, D.; Bonca, J.; Vidmar, L. Dissociation of a Hubbard-Holstein bipolaron driven away from equilibrium by a constant electric field. *Physica B* **2012**, *85*, 144304.
(31) Lakhno, V. D.; Korshunova, A. N. Electron motion in a Holstein molecular chain in an electric field. *Eur. Phys. J. B* **2011**, *79*, 147−151.
(32) Campbell, D. K.; Bishop, A. R.; Fesser, K. Polarons in quasi-one-dimensional systems. *Phys. Rev. B* **1982**, *26*, 6862−6874.
(33) Bishop, A. R.; Campbell, D. K.; Lomdahl, P. S.; Horovitz, B.; Phillpot, S. Non-linear dynamics, breathers and photoinduced absorption in polyacetylene. *Synth. Met.* **1984**, *9*, 223−239.
(34) Su, W. P.; Schrieffer, J. R.; Heeger, A. J. Solitons in polyacetylene. *Phys. Rev. Lett.* **1979**, *42*, 1698−1701.
(35) Brazovskii, S. A.; Kirova, N. N. Excitons, polarons, and bipolarons in conducting polymers. *Sov. Phys. JETP Lett.* **1981**, *33*, 4−8.
(36) Peierls, R. E. *Quantum Theory of Solids*; Oxford University Press: Oxford, 1974.
(37) Flytzanis, N.; Ivic, Z.; Malomed, B. A. Diffusion of randomly driven solitons in molecular chains. *Europhys. Lett.* **1995**, *30*, 267−272.
(38) Flytzanis, N.; Ivic, Z.; Malomed, B. A. Radiation emission by a polaron in a molecular chain. *J. Phys. Condens. Matter.* **1995**, *7*, 7843−7850.
(39) Shampine, L. F.; Reichelt, M. W. The MATLAB Ode suite. *SIAM J. Sci. Comput.* **1997**, *18*, 1−22.
(40) Heeger, A. J.; Kivelson, S.; Schrieffer, J. R.; Su, W. P. Solitons in conducting polymers. *Rev. Mod. Phys.* **1988**, *60*, 781−850.
(41) Fftw. http://www.fftw.org (accessed June 6, 2018).
(42) Roncaratti, L. F.; Gargano, R.; e Silva, G. M. Theoretical Temperature Dependence of the Charge-Carrier Mobility in Semiconducting Polymers. *J. Phys. Chem. A* **2009**, *113*, 14591−14594.


https://doi.org/10.1021/acsomega.3c05078
*ACS Omega* 2023, 8, 40456−40462